

# Skyrmions and Anomalous Hall Effect in a Dzyaloshinskii-Moriya Spiral Magnet

Su Do Yi,<sup>1</sup> Shigeki Onoda,<sup>2</sup> Naoto Nagaosa,<sup>3,4</sup> and Jung Hoon Han<sup>1,\*</sup>

<sup>1</sup>*Department of Physics, BK21 Physics Research Division,  
Sungkyunkwan University, Suwon 440-746, Korea*

<sup>2</sup>*Condensed Matter Theory Laboratory, RIKEN, 2-1, Hirosawa, Wako 351-0198, Japan*

<sup>3</sup>*Department of Applied Physics, The University of Tokyo,  
7-3-1, Hongo, Bunkyo-ku, Tokyo 113-8656, Japan*

<sup>4</sup>*Cross Correlated Materials Research Group, Frontier Research System,  
Riken, 2-1 Hirosawa, Wako, Saitama 351-0198, Japan*

(Dated: June 7, 2018)

Monte Carlo simulation study of a classical spin model with Dzyaloshinskii-Moriya interaction and the spin anisotropy under the magnetic field is presented. We found a rich phase diagram containing the multiple spin spiral (or skyrme crystal) phases of square, rectangular, and hexagonal symmetries in addition to the spiral spin state. The Hall conductivity  $\sigma_{xy}$  is calculated within the  $sd$  model for each of the phases. While  $\sigma_{xy}$  is zero in the absence of external magnetic field, applying a field strength  $H$  larger than a threshold value  $H_c$  leads to the simultaneous onset of nonzero chirality and Hall conductivity. We find  $H_c = 0$  for the multiple spin spiral states, but  $H_c > 0$  for a single spin spiral state regardless of the field orientation. Relevance of the present results to MnSi is discussed.

PACS numbers: 75.10.Hk, 75.10.Jm

Spiral magnets due to the Dzyaloshinskii-Moriya (DM) interaction are attracting recent intense attention. MnSi is one such prominent example of a metallic chiral ferromagnet whose magnetic[1–3] and transport[4–6] properties have been thoroughly studied over several decades. Also the spiral magnet is a promising laboratory to study the important issue of the relationship between the non-trivial spin textures and the quantum electronic transport, since the non-collinear spin configurations can be easily realized in such magnets. Indeed, Lee *et al.* found the novel anomalous Hall effect (AHE) in a certain region of the pressure-temperature phase diagram of MnSi recently[5, 6]. Several calculations have pointed out a close connection between the spin chirality derived from the non-collinear spin ordering, the Berry phase associated with it, and the anomalous Hall effect which arises as a consequence[7–10].

The purpose of this paper is twofold. First, we address the possible phase diagram of a spiral magnet from a microscopic model that includes the DM interaction and spin anisotropy. The phase diagram in the plane of spin anisotropy-magnetic field including the multiple spin spiral or Skyrmion crystal phase of square, rectangular, and hexagonal symmetries is revealed. The anomalous Hall conductivity is calculated for a model of conduction electrons coupled to the spins via the double exchange interaction, and the relevance of Skyrmion spin texture on the Hall transport is studied. In this way, a clear and consistent connection is drawn between the underlying topological spin structure, and its manifestation in an anomalous Hall transport.

A continuum Hamiltonian written by Bak and Jensen for a prototypical chiral magnet MnSi some years ago[11] is adapted to a lattice spin model consisting of the ferromagnetic exchange ( $J$ ), DM interaction ( $K$ ), anisotropy

( $A_1$  and  $A_2$ ), and the Zeeman energy ( $H$ ):

$$\begin{aligned}
 H_S = & -J \sum_{\mathbf{r}} \mathbf{S}_{\mathbf{r}} \cdot (\mathbf{S}_{\mathbf{r}+\hat{x}} + \mathbf{S}_{\mathbf{r}+\hat{y}} + \mathbf{S}_{\mathbf{r}+\hat{z}}) \\
 & -K \sum_{\mathbf{r}} (\mathbf{S}_{\mathbf{r}} \times \mathbf{S}_{\mathbf{r}+\hat{x}} \cdot \hat{x} + \mathbf{S}_{\mathbf{r}} \times \mathbf{S}_{\mathbf{r}+\hat{y}} \cdot \hat{y} + \mathbf{S}_{\mathbf{r}} \times \mathbf{S}_{\mathbf{r}+\hat{z}} \cdot \hat{z}) \\
 & + A_1 \sum_{\mathbf{r}} \left( (S_{\mathbf{r}}^x)^4 + (S_{\mathbf{r}}^y)^4 + (S_{\mathbf{r}}^z)^4 \right) \\
 & - A_2 \sum_{\mathbf{r}} \left( S_{\mathbf{r}}^x S_{\mathbf{r}+\hat{x}}^x + S_{\mathbf{r}}^y S_{\mathbf{r}+\hat{y}}^y + S_{\mathbf{r}}^z S_{\mathbf{r}+\hat{z}}^z \right) - \mathbf{H} \cdot \sum_{\mathbf{r}} \mathbf{S}_{\mathbf{r}}.
 \end{aligned} \tag{1}$$

We take a cubic lattice structure rather than the full B20 lattice structure of MnSi[12].

Without the anisotropy terms and the magnetic field,  $H_S$  favors the spiral spin (SS) ground state in which the spiral spins lie in a plane orthogonal to the propagation vector  $\mathbf{k}$ :  $\mathbf{S}_{\mathbf{r}} \sim \mathbf{S}_{\mathbf{k}} e^{i\mathbf{k}\cdot\mathbf{r}} + \mathbf{S}_{\mathbf{k}}^* e^{-i\mathbf{k}\cdot\mathbf{r}}$ ,  $\mathbf{S}_{\mathbf{k}} \cdot \mathbf{k} = 0$ . The  $\mathbf{k}$  stretches along the [111] ([11] in 2D) direction with the magnitude  $k = |\mathbf{k}|$  fixed by  $\tan k = (K/J)(1/\sqrt{d})$ ,  $d$  being the spatial dimension. The pitch of the helix can be very long compared to lattice spacing due to the small  $K/J$  ratio in a material. Under high pressure there is also experimental evidence for the realization of a phase with multiple ordering vectors[3]. Throughout this paper we denote such a multiple- $\mathbf{k}$  spin structure as Skyrme crystal (SC). The reason for the nomenclature will become transparent shortly.

Monte Carlo (MC) simulated annealing procedure was employed to work out the ground states for varying anisotropy strengths ( $A_1, A_2$ ) and the field strength  $H$  oriented along the  $z$ -direction:  $\mathbf{H} = H\hat{z}$ . Some simplifications were made to save the computational cost. First, a 2D rather than the 3D lattice was used. Because the

realistic modulation period is very large and difficult to simulate, we also choose the ratio  $K/J = 2\pi/6$  (Hereafter we will take  $J \equiv 1$ ) which would give  $k = 2\pi/6$  in 2D without the anisotropy. Calculations were mostly carried out for  $18 \times 18$  lattice, with occasional checks on a  $30 \times 30$  lattice to ensure consistency.  $2 \times 10^5$  MC steps were used at each temperature in the annealing process. It turns out that the same ground state is found over a widely different choices of  $A_1$ , and here we present all the results for  $A_1 = 0.5$  without loss of generality. Once the ground state has been obtained for a given  $A_2$  and  $H$ , we analyze its structure by making the Fourier transform  $\langle \mathbf{S}_{\mathbf{k}} \rangle = \sum_{\mathbf{r}} \langle \mathbf{S}_{\mathbf{r}} \rangle e^{-i\mathbf{k} \cdot \mathbf{r}}$  of the averaged MC configurations  $\langle \mathbf{S}_{\mathbf{r}} \rangle$ , and looking at the intensity profile  $|\langle \mathbf{S}_{\mathbf{k}} \rangle|^2$ . A sharper spectral feature is obtained in this way than by taking the average of the individual intensities,  $\langle |\mathbf{S}_{\mathbf{k}}|^2 \rangle$ .

A pair of sharp peaks are obtained at  $\pm \mathbf{k}$  for a single SS, where  $\mathbf{k} = (k, k)$ . Each spin spiral has a right-handed helicity consistent with the sign of  $K > 0$ . When  $A_2$  is sufficiently large, one finds the SC phase given as the superposition of two pairs of spin spirals, with modulation vectors at  $(\pm k, 0)$  and  $(0, \pm k)$ . Depending on whether the Bragg intensities  $|\langle \mathbf{S}_{\mathbf{k}} \rangle|^2$  are the same or different for the two pairs, we denote them as  $SC_1$  (non-identical) or  $SC_2$  (identical). In practice  $SC_1$  is fragile, occupying only a tiny fraction of the phase diagram. A third class of SC state is found when the field strength in exceed of a certain threshold value  $H_c$  is applied to the SS phase. This state, denoted  $SC_h$ , is characterized by three sets of modulation vectors which are related by  $120^\circ$  rotations. We later point out that this phase, and  $SC_1$  and  $SC_2$  phases under nonzero magnetic field, also carries a nonzero uniform spin chirality and anomalous Hall conductivity. The low temperature schematic phase diagram as obtained from examination of the Bragg intensity  $|\langle \mathbf{S}_{\mathbf{k}} \rangle|^2$  is shown in Fig. 1.

Although the details of the phase transitions among the phases deserves further, more careful study in the future work, we can make some qualitative statements based on symmetry. The transition from SS to  $SC_h$  and SS to  $SC_1$  are necessarily first-order, while  $SC_1 \leftrightarrow SC_2$  can be second-order. In going from  $SC_h$  or  $SC_2$  to the fully spin-polarized (SP) state at high field, the intensity of Bragg peaks gradually diminishes, leaving only the  $\mathbf{k} = 0$  peak in the SP phase.

The projection of spin patterns onto the  $xy$  plane is displayed in Fig. 2 for the three Skyrme crystal states. We introduce the local chirality  $\chi_{\mathbf{r}}$  at the lattice site  $\mathbf{r}$  as

$$8\pi\chi_{\mathbf{r}} = \mathbf{S}_{\mathbf{r}} \cdot (\mathbf{S}_{\mathbf{r}+\hat{x}} \times \mathbf{S}_{\mathbf{r}+\hat{y}}) + \mathbf{S}_{\mathbf{r}} \cdot (\mathbf{S}_{\mathbf{r}-\hat{x}} \times \mathbf{S}_{\mathbf{r}-\hat{y}}). \quad (2)$$

It is well known that a single localized Skyrmion would give the uniform chirality  $\chi = \sum_{\mathbf{r}} \chi_{\mathbf{r}}$  equal to unity. Plots of  $\chi_{\mathbf{r}}$  in Fig. 2 clearly display the presence of Skyrmion (bright) and anti-Skyrmion (dark) regions. The skyrmion density map is largely one-dimensional for

$SC_1$ , checkerboard-like for  $SC_2$ , and hexagonal for  $SC_h$ . The uniform chirality  $\chi$  was zero for the states obtained at zero field.

Expanding  $\mathbf{S}_{\mathbf{r}} = \sum_{\mathbf{k}} \mathbf{S}_{\mathbf{k}} e^{i\mathbf{k} \cdot \mathbf{r}}$ , the uniform chirality reads  $\chi = \sum_{\mathbf{k}_1, \mathbf{k}_2} \mathbf{S}_{\mathbf{k}_1 + \mathbf{k}_2}^* \cdot \mathbf{S}_{\mathbf{k}_1} \times \mathbf{S}_{\mathbf{k}_2} \cos(k_{1x} + k_{2y})$ . Our calculation explicitly shows that this quantity is zero without the magnetic field. With the field on there appears the  $\mathbf{k} = 0$  component of spin,  $\mathbf{S}_0 \propto \mathbf{H}$ . One might think that a non-zero chirality results from  $\chi \sim \mathbf{H} \cdot \sum_{\mathbf{k}} \mathbf{S}_{\mathbf{k}} \times \mathbf{S}_{-\mathbf{k}}$ , but since  $\mathbf{S}_{\mathbf{k}} \times \mathbf{S}_{-\mathbf{k}} \sim i\mathbf{k}$  and thus  $\mathbf{S}_{\mathbf{k}} \times \mathbf{S}_{-\mathbf{k}} + \mathbf{S}_{-\mathbf{k}} \times \mathbf{S}_{\mathbf{k}} = 0$ , the chirality contribution from a given spin spiral is zero. Rather, we find that the uniform chirality is induced in the  $SC_1$  and  $SC_2$  phases due to the appearance of additional Bragg peaks at  $\mathbf{S}_{\pm \mathbf{k}_x \pm \mathbf{k}_y}$ ,  $\mathbf{k}_x = (k, 0)$  and  $\mathbf{k}_y = (0, k)$ , and the nonzero value of the triple product such as  $\mathbf{S}_{\mathbf{k}_x + \mathbf{k}_y}^* \cdot \mathbf{S}_{\mathbf{k}_x} \times \mathbf{S}_{\mathbf{k}_y}$ . Why the  $\mathbf{S}_{\mathbf{k}_x + \mathbf{k}_y}$  component appears with  $H$  can be understood from a Ginzburg-Landau theory which should contain, on symmetry grounds, a quartic coupling such as  $(\mathbf{S}_{\mathbf{k}_1} \cdot \mathbf{S}_{\mathbf{k}_2})(\mathbf{S}_{\mathbf{k}_3} \cdot \mathbf{S}_{\mathbf{k}_4})$ . With the appearance of  $\mathbf{S}_0 \sim \mathbf{H}$ , the coupling becomes  $(\mathbf{S}_{\mathbf{k}_x} \cdot \mathbf{S}_{\mathbf{k}_y})(\mathbf{S}_{\mathbf{k}_x + \mathbf{k}_y}^* \cdot \mathbf{H})$ . Since  $\mathbf{S}_{\mathbf{k}_x} \cdot \mathbf{S}_{\mathbf{k}_y}$  is already nonzero in the SC phase, it implies the appearance of a linear term in  $S_{\mathbf{k}_x + \mathbf{k}_y}$  which will lead to the condensation of  $S_{\mathbf{k}_x + \mathbf{k}_y}$  order and  $\chi$  proportional to  $H$ . The numerical results shown in Fig. 3 confirm the linear growth of  $\chi$  with  $H$ . For  $SC_h$ , the uniform chirality is found to arise from the nonzero triplet product  $\chi \sim \mathbf{S}_{\mathbf{k}_1} \cdot \mathbf{S}_{\mathbf{k}_2} \times \mathbf{S}_{\mathbf{k}_3}$ , where the three independent modulation vectors form  $\mathbf{k}_1 + \mathbf{k}_2 + \mathbf{k}_3 = 0$ .

For field oriented away from the  $z$ -axis, the Ginzburg-Landau argument would continue to predict the presence of a linear- $H$  dependence of the chirality in the  $SC_1$  and  $SC_2$  phases and lack therefore for the SS phase. Both these predictions are confirmed by the numerical calculations. Some check was made on the finite-temperature behavior, using the thermal-averaged intensity  $|\langle \mathbf{S}_{\mathbf{k}} \rangle|^2$  was used as a measure of magnetic ordering. The largest intensity in  $|\langle \mathbf{S}_{\mathbf{k}} \rangle|^2$  among all values of  $\mathbf{k}$  decreased continuously until it reaches zero at the critical temperature. There was no clear evidence for the existence of an intermediate phase.

Having studied the magnetic phase diagram, we turn to the coupling of the local moments to the conduction electrons that would result in the anomalous Hall effect. We adopt the  $sd$  Hamiltonian

$$H = -t \sum_{\mathbf{r}\mathbf{r}'\sigma} c_{\mathbf{r}\sigma}^+ c_{\mathbf{r}'\sigma} - \lambda \sum_{\mathbf{r}} \mathbf{S}_{\mathbf{r}} \cdot c_{\mathbf{r}\alpha}^+ (\sigma)_{\alpha\beta} c_{\mathbf{r}\beta}, \quad (3)$$

with the moment distribution  $\{\mathbf{S}_{\mathbf{r}}\}$  obtained from previous MC calculation. The intrinsic anomalous Hall conductivity  $\sigma_{xy}$  is calculated from

$$\sigma_{xy} = \frac{2\pi}{L^2} \sum_{m \neq n} \frac{f_n - f_m}{\eta^2 + (\varepsilon_m - \varepsilon_n)^2} \text{Im} \left( \langle m | J_x | n \rangle \langle n | J_y | m \rangle \right) \quad (4)$$

expressed in units of  $e^2/h$ . The sum  $\sum_{m \neq n}$  extends over all non-identical pairs of single-particle eigenstates of Eq. (3),  $f_m$  is the Fermi function  $1/(e^{\beta\varepsilon_m} + 1)$ , and  $L^2$  gives the number of lattice sites.  $J_x$  and  $J_y$  are the current operators. The same temperature  $T$  is used both in the Monte Carlo generation of sample spin configurations, and in evaluating  $\sigma_{xy}$ . Thermal average  $\langle \sigma_{xy} \rangle$  was taken over 100 MC-generated spin configurations. The relaxation rate  $\eta = 0.1$ , and the  $sd$  coupling  $\lambda = 1$  were used in the calculation, with similar results at other parameter choices. Since the relativistic spin-orbit coupling term is absent in Eq. (3), the nonzero Hall conductivity we will report below can only be due to the topological Berry phase effects.

We find  $\langle \sigma_{xy} \rangle = 0$  for all the spin configurations at all temperatures when  $H = 0$ . For finite fields, the onset of nonzero  $\langle \sigma_{xy} \rangle$  and nonzero  $\chi$  coincided almost perfectly, confirming the earlier theoretical anticipation that an unconventional anomalous Hall conductivity arises as a consequence of uniform chirality  $\chi$  being nonzero[7, 8, 10]. We also verified that the relation between  $\langle \sigma_{xy} \rangle$  and  $\chi$  are linear when both quantities are sufficiently small. Such a close tie between  $\chi$  and  $\langle \sigma_{xy} \rangle$  suggests that measurement of  $\sigma_{xy}$  in a given material can be used as an effective probe of the underlying spin structure. For instance, linear rise of  $\sigma_{xy}$  with the magnetic field would be consistent with the Skyrme crystal spin structure, but not with the spiral spin structure.

The field dependence of uniform magnetization  $M$ , uniform chirality  $\chi$ , and  $\langle \sigma_{xy} \rangle$  are displayed in Fig. 3 for several temperatures. Under the full polarization  $M = 1$ ,  $\langle \sigma_{xy} \rangle$  and  $\chi$  naturally must go to zero, resulting in the characteristic dome shape of the  $\langle \sigma_{xy} \rangle$  curve. A roughly linear relationship  $\sigma_{xy} \propto H \propto M$  exists in both SC<sub>1</sub> and SC<sub>2</sub> for small  $M$ . The slope  $\sigma_{xy}/H$  decreases gradually as the temperature rises. The low-temperature  $\sigma_{xy}$  can reach up to  $\approx 10e^2/h$ , similar to the value reported in the model calculation by Metalidis and Bruno[9].

Now we discuss the possible relevance of our results to MnSi. Several mechanisms for de-stabilizing the SS order in a chiral magnet have been proposed[13–16]. Tewari *et al.* argued for the existence of a chiral liquid phase on the high pressure side of MnSi, *i.e.* a non-magnetic phase with nonzero  $\langle \psi_{\mathbf{r}} \rangle$ ,  $\psi_{\mathbf{r}}$  being the chiral order parameter  $\psi_{\mathbf{r}} = \mathbf{S}_{\mathbf{r}} \cdot \nabla \times \mathbf{S}_{\mathbf{r}}$ . Provided that one can associate their pressure variable with  $A_2$  in our model, we find the skyrme crystal phase characterized by  $\chi_{\mathbf{r}} = \mathbf{S}_{\mathbf{r}} \cdot (\partial_x \mathbf{S}_{\mathbf{r}} \times \partial_y \mathbf{S}_{\mathbf{r}})$  in place of their chiral liquid order. Robler *et al.*[15] considered a Ginzburg-Landau model which supports a Skyrme crystal phase at the intermediate temperature range between the low-temperature SS

and the high-temperature paramagnet. Our model in contrast exhibits the skyrme crystal phase at *low temperature*, driven by the *large anisotropy term* comparable to  $J$  and/or  $K$ .

Several features of the experiments on MnSi might be understood within the framework of our model. The first-order change with  $A_2$  in going from SS to SC phase and the re-orientation of the primary ordering vector from [11] to [10] direction in our model are consistent with the first-order collapse of  $T_c$  at the critical pressure and the re-orientation of the main Bragg peak from [111] to [110] in MnSi, respectively[3]. The appearance of an anomalous Hall signal on the high pressure side[6] and over a finite temperature and field segments of the phase diagram might indicate the realization of a topologically nontrivial spin structure, according to the close tie between anomalous Hall conductivity and nonzero spin chirality found in our study. It is also tempting to associate the recently observed hexagonal Bragg spots in the so-called A-phase of MnSi[18] with the SC<sub>h</sub> found in our spin model. Further measurement of the anomalous Hall conductivity in the same phase will help clarify the connection. The highly nonlinear threshold behavior of  $\sigma_{xy}$  in the SS phase has not yet been clearly resolved in existing measurements of ordinary Hall effect by Lorentz force or the anomalous Hall effect on MnSi[5, 6].

We close with a caveat that the correspondence between our theory and experiments on MnSi rests on the physical assumption that increasing pressure does lead to the increase of  $A_2$  over other energy scales. Whether the Mn orbitals responsible for the localized moments in MnSi will give rise to such an interaction, and if the pressure does have an effect on  $A_2$  remains a subject for future consideration. Nevertheless, the predicted field dependence of  $\sigma_{xy}$  on the underlying spin structure is independent of the microscopic spin model being used.

N. N. is supported by Grant-in-Aids under the grant numbers 16076205, 17105002, 19019004, and 19048015 from the Ministry of Education, Culture, Sports, Science and Technology of Japan. S.O. is supported by Grants-in-Aid for Scientific Research (No. 20029006 and No. 20046016) from the MEXT of Japan. H. J. H. is supported by the Korea Research Foundation Grant (KRF-2008-521-C00085, KRF-2008-314-C00101) and in part by the Asia Pacific Center for Theoretical Physics.

---

\* Electronic address: hanjh@skku.edu

- [1] Y. Ishikawa, K. Tajima, D. Bloch, and M. Roth, Solid State Commun. **19**, 525 (1976).
- [2] C. Thessieu *et al.*, J. Phys: Condens. Matter **9**, 6677 (1997).
- [3] C. Pfeiderer *et al.*, Nature **427**, 227 (2004).
- [4] C. Pfeiderer *et al.*, Phys. Rev. B **55**, 8330 (1997); C. Pfeiderer, S. R. Julian, and G. G. Lonzarich, Nature **414**,

- 427 (2001); N. Doiron-Leyraud, *et al.*, *Nature* **425**, 595 (2003).
- [5] Minhyea Lee, Y. Onose, Y. Tokura, and N. P. Ong, *Phys. Rev. B* **75**, 172403 (2007).
- [6] Minhyea Lee, W. Kang, Y. Onose, Y. Tokura, and N. P. Ong, arXiv:0811.3146v2.
- [7] Jinwu Ye *et al.*, *Phys. Rev. Lett.* **83**, 3737 (1999).
- [8] S. H. Chun *et al.*, *Phys. Rev. Lett.* **84**, 757 (2000); *Phys. Rev. B* **63**, 184426 (2001).
- [9] G. Metalidis and P. Bruno, *Phys. Rev. B* **74**, 045327 (2006).
- [10] Naoto Nagaosa, *J. Phys. Soc. Jpn.* **75**, 042001 (2006).
- [11] Per Bak and M. Høgh Jensen, *J. Phys. C* **13**, L881 (1980).
- [12] John M. Hopkinson and Hae-Young Kee, *Phys. Rev. B* **79**, 014421 (2009).
- [13] S. Tewari, D. Belitz, and T. R. Kirkpatrick, *Phys. Rev. Lett.* **96**, 047207 (2006).
- [14] B. Binz, A. Vishwanath, and V. Aji, *Phys. Rev. Lett.* **96**, 207202 (2006); B. Binz and A. Vishwanath, *Phys. Rev. B* **74**, 214408 (2006).
- [15] U. K. Robler, A. N. Bogdanov, and C. Pfeiderer, *Nature* **442**, 797 (2006).
- [16] Inga Fischer, Nayana Shah, and Achim Rosch, *Phys. Rev. B* **77**, 024415 (2008).
- [17] B. Binz, A. Vishwanath, *Physica B* **403**, 1336 (2008).
- [18] S. Mühlbauer *et al.*, *Science* **323**, 915 (2009).

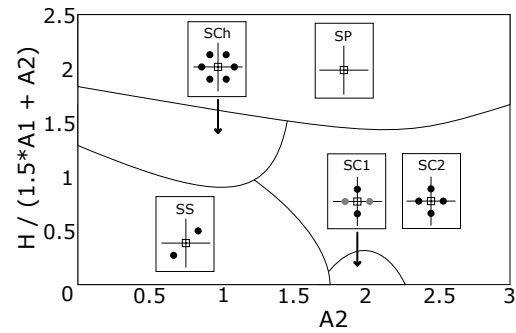


FIG. 1: (color online) Low temperature ( $T = 0.01$ ) phase diagram of the spin model in Eq. (1) with  $K = \sqrt{6}$ ,  $A_1 = 0.5$ , and  $\mathbf{H} = H\hat{z}$ . Phase boundaries are drawn on the basis of MC simulations at a large number of  $(A_2, H)$  locations. Spin configurations are abbreviated as SS (spiral spin), and SC (spin crystal). Full spin polarization (SP) results at high field. The spin crystal phases are further classified as  $SC_1$  (unequal Bragg intensities),  $SC_2$  (equal Bragg intensities), and  $SC_h$

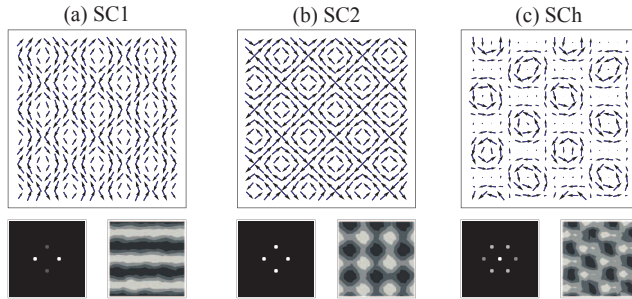


FIG. 2: (color online) A plot of the spin configuration projected on the  $xy$  plane ( $S_i^x, S_i^y$ ) in the three spin crystal ground states: (a) SC<sub>1</sub> at  $(A_1, A_2, H) = (0.5, 2.0, 0.0)$ , (b) SC<sub>2</sub> at  $(A_1, A_2, H) = (0.5, 3.0, 0.0)$ , and (c) SC<sub>h</sub> at  $(A_1, A_2, H) = (0.5, 0.0, 2.0)$ . At the bottom left of each figure are the plots of the Bragg intensity  $|\langle \mathbf{S}_{\mathbf{k}} \rangle|^2$  showing two (SC<sub>1</sub>, SC<sub>2</sub>) and three (SC<sub>h</sub>) sets of modulation vectors. Shown at the bottom right are the plots of the local chirality  $\chi_r$ . Bright (dark) regions correspond to Skyrmions (anti-Skyrmions).

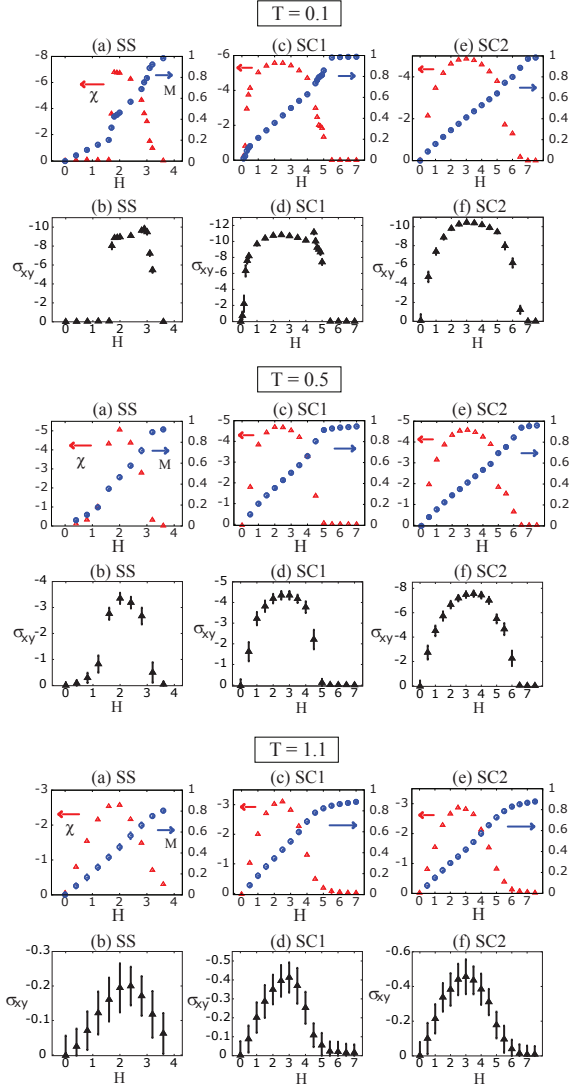


FIG. 3: (color online) Upper panels: Plot of uniform magnetization  $M$  (blue circle) and uniform chirality  $\chi$  (red triangle) with varying field strength  $H$ ,  $\mathbf{H} = H\hat{z}$ , for (a) SS at  $(A_1, A_2) = (0.5, 0.0)$ , (c) SC<sub>1</sub> at  $(A_1, A_2) = (0.5, 2.0)$ , and (e) SC<sub>2</sub> at  $(A_1, A_2) = (0.5, 3.0)$ , at three temperatures  $T = 0.1$  (top six figures),  $0.5$  (middle), and  $1.1$  (bottom). Lower panels:  $\langle \sigma_{xy} \rangle$  averaged over 100 MC-generated spin configurations are shown in (b), (d), and (f) at the corresponding